Polymer Journal, Vol. 39, No. 11, pp. 1085–1097 (2007)

SPECIAL ISSUES -PROGRESS IN STRUCTURE ANALYSES OF POLYMERIC MATERIALS BY SYNCHROTRON RADIATION AND NEUTRON BEAM-
REVIEW ARTICLES

Quantum Beam Studies on Polymer Crystallization under Flow

Toshiji KANAYA,[1,†] Go MATSUBA,[1] Yoshiko OGINO,[2]
Nobuaki TAKAHASHI,[3] and Koji NISHIDA[1]

[1]*Institute for Chemical Research, Kyoto University, Uji 611-0011, Japan*
[2]*Department of Polymer Chemistry, Kyoto University, Katsura, Kyoto 615-8510, Japan*
[3]*J-PARC Center, Japan Atomic Energy Agency, 2-4 Shirakatashirane, Tokai 319-1195, Japan*

(Received July 13, 2007; Accepted August 9, 2007; Published September 26, 2007)

ABSTRACT: One of the longstanding issues in polymer science is crystallization of polymers under flow, especially formation of the so-called shish-kebab. Recent progress in quantum beam technology shed light on the substantial nature in the shish-kebab formation. In this paper we review our recent experiments on polymer crystallization under flow using time-resolved depolarized light scattering, small-angle and wide-angle X-ray scattering and small-angle neutron scattering in a wide spatial scale from 0.1 nm to several tens μm. These studies revealed that the shish-kebab formation is governed by a competition between the crystallization rate and the chain relaxation rate. Small-angle neutron scattering study on an elongated blend of deuterated low molecular weight and protonated ultra-high molecular weight polyethylenes showed that a long cylindrical object 2 μm in diameter and 12 μm in length was formed from deformed network of ultra-high molecular weight chains, which included three shishs (or extended chain crystals) 9 nm in diameter. [doi:10.1295/polymj.PJ2007098]

KEY WORDS Quantum Beam / Polymer Crystallization / Flow / Shish-Kebab / Hierarchic Structure / X-ray Scattering / Neutron Scattering /

In polymer processing molten polymers crystallize under various kinds of flows such as shear flow, elongational flow and mixed flow, and the final structure and morphology are strongly affected by the flow conditions.[1–3] In order to obtain desired properties of polymers it is necessary to control the final structure of polymers in the processing. Therefore, many researches have been carried out on polymer crystallization under flows for many decades to elucidate the crystallization mechanism and control the final structure. One of the famous issues in the research filed is structure and formation mechanism of the so-called shish-kebab, which consists of long central fiber core (shish) surrounded by lamellar crystalline structure (kebab) periodically attached along the shish, and it is believed that the shish-kebab structure is a structure origin of ultra-high strength and ultra-high modulus fibers.[4–10] This is one of the reasons why so many studies have been performed on the structure and the formation mechanism of shish-kebab. In spite of the great efforts there are still many unsolved problems in the shish-kebab. For example, even size of shish-kebab structure is not still fully understood. About 30 years ago, Keller and co-workers observed shish-kebab structure in polyethylene (PE) using transmission electron microscope (TEM),[7–11] showing shish of ~10 nm in diameter and several μm in length. This has been assigned to extended chain crystal. On the other hand, large and long objects with diameter of several μm aligned along the flow direction are often observed in some polymers[24,28] using optical microscope (OM). This long object is apparently similar to the shish structure but the spatial scale is very different. It must include the kebab inside judging from the spatial scale. These observations suggest that shish-kebab has hierarchic structure in a wide spatial scale. However, few papers did not deal with the hierarchic structure of the shish-kebab structure. One of the reasons is difficulty to study the shish-kebab structure in a wide spatial range simultaneously, in addition, kebab structure is overlapped on the shish structure, so that it is not easy to distinguish the shish from the kebab.

Recently, quantum beam technology has been developed to provide well-controlled laser beam, synchrotron radiation (SR) X-ray beam, and high flux neutron beam. On the basis of the advanced technology new experiments have been performed on polymer crystallization under flow using time resolved small-angle and wide-angle X-ray scattering (SAXS and WAXS),[12–22] time resolved small-angle light scatter-

[†]To whom correspondence should be addressed (Tel: +81-774-38-3140, Fax: +81-774-38-3146, E-mail: kanaya@scl.kyoto-u.ac.jp).

ing (SALS)[23–28] and optical measurements,[29–32] providing fruitful information on the formation mechanism of shish-kebab structure. In this paper we will review our recent experiments on polymer crystallization using quantum beam technology such as time-resolved depolarized light scattering (DPLS), time-resolved SAXS, time-resolved WAXS, and small-angle neutron scattering (SANS). The review includes two topics. The first one is the crystallization of isotactic polypropylene (iPP) under shear flow. In the study we focus on effects of the shear rate and shear strain on the shish-kebab formation in a wide spatial scale from Å to several tens μm. We observe the shish formation, the kebab formation and the crystalline lattice formation individually using DPLS, SAXS and WAXS, respectively, elucidating that the relation between the shish formation and the kebab formation. In the second topic we investigate effects of ultra-high molecular component on the formation of shish-kebab of polyethylene (PE). Some reports have already shown that the ultra-high molecular weight component enhanced the shish-kebab formation, but the data were not quantitative. In this work we investigate the effects of the ultra-high molecular weight component on the shish formation as a function of the concentration of ultra-high molecular weight component and the crystallization temperature, revealing an important role of entanglements of the ultra-high molecular weight chains. In SANS measurements we investigate hierarchic structure of shish-kebab using a deuterium labeling method. The results demonstrate for the first time that large row structure 2 μm in diameter and 12 μm in length, which is formed from deformed network of ultra-high molecular weight chains, includes only three shishs (extended chain crystals).

EXPERIMENTAL

Materials

Isotactic polypropylene (iPP): We used isotactic polypropylene (iPP) with the molecular weight M_w = 238,000 and the polydispersity $M_w/M_n = 5.1$, where M_w and M_n are the weight-average and number-average molecular weights, respectively. The iPP was synthesized using metallocene catalysis. Pentad tacticity determined by NMR measurements was *mmmm* = 0.974. The nominal melting temperature of the iPP determined by DSC measurements was 149 °C at the heating rate of 20 °C/min.

Polyethylene (PE): We used ultra-high molecular weight (UHMW) polyethylenes (PE) with M_w = 2,000,000 and $M_w/M_n = 12$ and low molecular weight (LMW) PE with M_w = 58,600 and M_w/M_n = 8.01 for DPLS and SAXS measurements. The nominal melting temperatures of the LMW and UHMW PEs determined by DSC measurements were 134 and 135 °C, respectively, at a heating rate of 20 °C/min. Two polyethylenes were blended in hot xylene to ensure the intimate mixing at the molecular level. The solution was quenched into ice water to precipitate as a gel, and it was vacuum-dried at 70 °C for 2 d and then hot-pressed at 165 °C for 5 min. For the SANS measurements, we used UHMW PE and LMW deuterated PE with M_w = 200,000 and $M_w/M_n = 5$, respectively. The UHMW PE is the same PE as in the DPLS and SAXS measurements. Strips of the blend film of UHMW hydrogenated PE (2.8 wt %) and LMW deuterataed PE (97.2 wt %), which was prepared in the same procedure as the DPLS samples, were elongated about 6 times at 133 °C just below the nominal melting temperature (= 135 °C) and quenched into ice water. The details of the sample preparation has been described elsewhere.[43]

DPLS Measurements

Two-dimensional (2D) depolarized light scattering (DPLS) measurements were carried out using a home-made apparatus with He-Ne laser (80 mW, wavelength $\lambda = 633$ nm) as a light source and a CCD camera with 2D screen as a detector system. The range of length of scattering vector Q in this experiment is 4×10^{-5} to 2.6×10^{-4} Å^{-1}, where Q is given by $Q = 4\pi \sin\theta/n\lambda$ (2θ and n being scattering angle and the refractive index, respectively). A Linkam CSS-450 high temperature shear cell was used for the DPLS measurements to control the temperature and the shear conditions. The temperature protocol for the DPLS experiments is shown in Figure 1 for PE: (a) heat up the polymer sample from room temperature to 165 °C at a rate of 30 °C/min, (b) hold at 165 °C for 5 min, (c) cool down to the crystallization temperature T_c = 129 °C at a rate of 30 °C/min, and (d) hold the temperature at 129 °C for the DPLS measurements. The polymer melt was subjected to pulse shear just after reaching the crystallization temperature T_c of 129 °C.

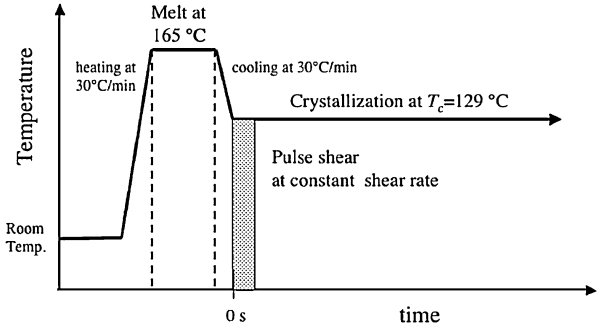

Figure 1. Temperature protocol for crystallization process of PE blend.

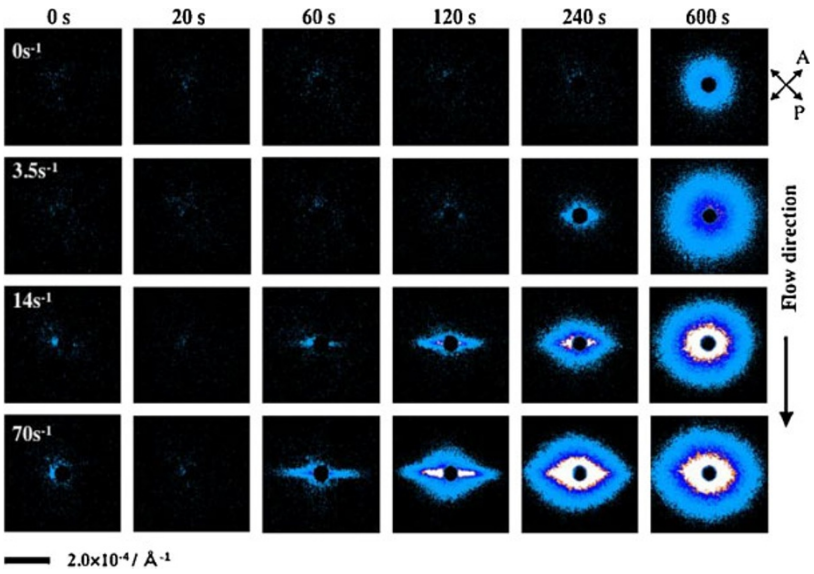

Figure 2. Time evolution of 2D DPLS patterns during crystallization process of iPP at 132 °C for various shear rates, $\dot{\gamma} = 0$, 3.5, 14 and 70 s^{-1}. (Reprinted from Ref. 28 with permission from American Chemical Society)

SAXS Measurements

SAXS measurements were carried out using apparatus at the beam line BL40B2 and BL45XU[33] in the SR facility, SPring-8, Nishiharima, and apparatus at the beam line BL-15A in Photon Factory, KEK, Tsukuba. A CCD camera (C4880: Hamamatsu Photonics K.K.) with an image intensifier was used as a detector system for the SAXS measurements. In the measurements we covered a Q range of 6×10^{-3} to 2×10^{-1} Å^{-1}. Here, Q is given by $Q = 4\pi \sin\theta/\lambda$. We also used U-SAXS machine with Bonse-Hart type camera (TRY-HV) to a low Q range of 1×10^{-5} to 8×10^{-3} Å^{-1}.

A Linkam CSS-450 high temperature shear cell was also used for the SAXS measurements to control the temperature and the shear conditions. The thin film sample was placed between two stainless plates with Kapton windows 50 μm thick. The temperature protocol was the same as in the DPLS measurements, but the pulse shear was applied at 30 °C above the crystallization temperature T_c.

SANS Measurements

SANS measurements were performed using three spectrometers. One is F-SANS spectrometer at JRR-3 reactor in Tokai with neutron focusing lens made of MgF_2 with diameter 30 mm, curvature radius 25 and thickness 10.5 mm. Using F-SANS, we can perform two dimensional measurements in a very low Q range from 1×10^{-4} to 10^{-2} Å^{-1}. We also used SANS-U spectrometer[34] at JRR-3 reactor in Tokai. In the SANS-U measurements, the scattering vector Q range was from 6×10^{-3} to 7×10^{-2} Å^{-1}. In addition, we used time-of-flight (TOF) SANS spectrometer SWAN[35] installed at a spallation pulse cold neutron source at KENS, Tsukuba, in order to extend the Q range up to 3 Å^{-1}. In this spectrometer we measure scattering intensity as a function of neutron wavelength λ as well as scattering angle 2θ. Hence, we can cover a very wide Q range from 10^{-2} to 3 Å^{-1} in the measurements. Combining all the data by three spectrometers we coverd a Q range from 10^{-4} to 3 Å^{-1} in this study. This wide Q range is a distinct feature of this experiment.

RESULTS AND DISCUSSION

Crystallization of iPP under Shear Flow

Depolarized Light Scattering. Time-resolved depolarized light scattering (DPLS) measurements were performed on the crystallization process of iPP at a crystallization temperature 132 °C for various shear rates, and the results are shown in Figure 2. Under the quiescent crystallization condition ($\dot{\gamma} = 0\,s^{-1}$), we observed isotropic scattering pattern after an induction period before nucleation of about 5 min. On the other hand, as the shear rate increased we observed anisotropic streak-like scattering pattern along the direction normal to the shear. This indicates that there are long scattering objects aligned along the flow direction, which must be the shish structure or the precursor of shish structure. In order to analyze the DPLS data we employed two measures. One is the anisotropy in the 2D scattering pattern, which is defined as a ratio of integrated intensity in the normal direction to the parallel one, termed degree of anisotropy. Another measure is the length of the induction period before the streak-like scattering appears in the direction

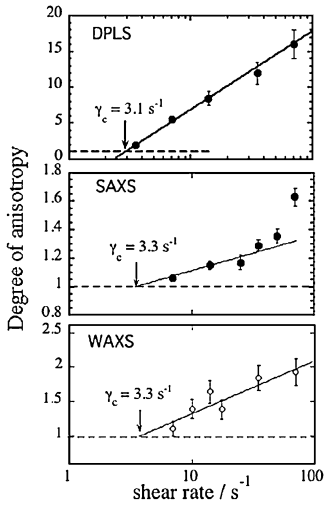

Figure 3. Degree of anisotropy for 2D DPLS, SAXS and WAXS patterns of iPP as a function of shear rate. Dashed lines in the figures show value of one.

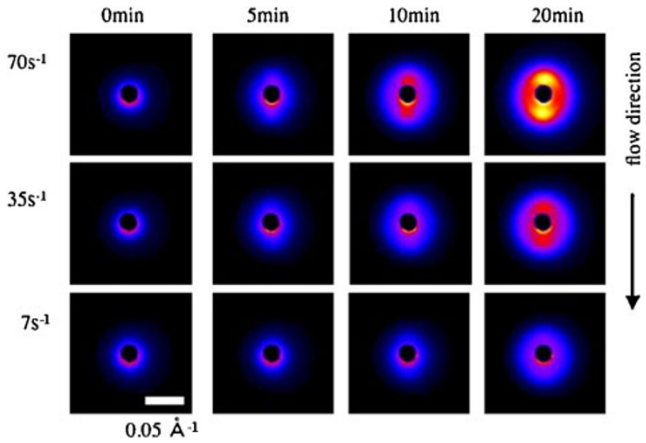

Figure 4. Time evolution of 2D SAXS patterns during crystallization process of iPP at 132 °C for various shear rates, $\dot{\gamma} = 7$, 35 and 70 s^{-1}. (Reprinted from Ref. 28 with permission from American Chemical Society)

normal to the flow. The former and the latter are measures of anisotropic structure formation and crystal nucleation rate, respectively.

The degree of anisotropy was plotted against logarithm of the shear rate in Figure 3 (upper), showing the linear relationship. The critical shear rate $\dot{\gamma}^*_{ani,DPLS}$ was evaluated to be $3.1 \pm 0.3\,s^{-1}$ by extrapolating the degree of anisotropy to unity. We also evaluated the critical shear rate for the induction period $\dot{\gamma}^*_{ind,DPLS}$ to be $\sim 1\,s^{-1}$ although the data was not shown here. The critical shear rate for the degree of anisotropy $\dot{\gamma}^*_{ani,DPLS}$ is larger than that for the induction period $\dot{\gamma}^*_{ind,DPLS}$. Similar results were reported for polyethylene.[26] The physical meaning of the finding will be discussed later after showing the SAXS and WAXS data. Next we performed time-resolved small-angle X-ray scattering measurements on the crystallization process of the same iPP in tens nm scale to see the formation process of the kebab.

Small-angle X-ray Scattering. Time-resolved small-angle X-ray scattering (SAXS) measurements were carried out on crystallization process of iPP under the same temperature and shear conditions as the DPLS. The observed time evolution of 2D SAXS patterns was shown in Figure 4 for the shear rates of 7, 35 and $70\,s^{-1}$. Under the quiescent condition, only isotropic scattering patterns were observed and the onset time of the scattering intensity is about 650 s after reaching the crystallization temperature T_c (= 132 °C). On the other hand, under the shear condition, the onset time of the scattering intensity is earlier than that under the quiescent condition and the scattering pattern is anisotropic. The anisotropic SAXS pattern is completely different from the DPLS one (see Figure 2), in which streak-like scattering appears in a direction normal to the flow. The observed two-spot SAXS pattern parallel to the flow direction must correspond to the distance between the lamellae (kebabs) periodically aligned along the shish structure. In order to analyze these SAXS data quantitatively we also used the onset time and the degree of anisotropy, which depended on the shear rate very much.

The degree of anisotropy for the 2D SAXS pattern was plotted in Figure 3 (middle) against logarithm of the shear rate. Assuming a linear relationship between the degree of anisotropy and the logarithm of the shear rate below $35\,s^{-1}$, we extrapolated the degree of anisotropy to unity to evaluate the critical shear rate $\dot{\gamma}^*_{ani,SAXS}$ to be $3.3 \pm 0.6\,s^{-1}$. We also evaluated the critical shear rate for the induction period $\dot{\gamma}^*_{ind,SAXS}$ to be $\sim 1\,s^{-1}$ although the data was not shown here. Similar to the DPLS result, the evaluate the critical shear rate $\dot{\gamma}^*_{ani,SAXS}$ is larger than the critical shear rate for the reduction in the induction period $\dot{\gamma}^*_{ind,SAXS}$ ($\sim 1\,s^{-1}$), and very close to that in the DPLS (the shish) $\dot{\gamma}^*_{ani,DPLS}$ ($= 3.1\,s^{-1}$). This must imply that the anisotropy of the kebab structure is dominated by the shish formation. This problem will be discussed later after showing the WAXS results.

Wide-angle X-ray Scattering. Time-resolved WAXS measurements were performed on the same iPP under the same temperature and shear conditions as the DPLS and SAXS measurements. In the WAXS measurements we observed the time evolution of the local crystalline structure in both of the shish and the kebab, particularly in the kebab because the amount of kebab was much larger than the shish. In order to see the anisotropy time evolution of 1D WAXS profiles normal and parallel to the shear direction are shown in Figure 5 for the shear rate of $70\,s^{-1}$.

The degree of anisotropy for the (040) diffraction

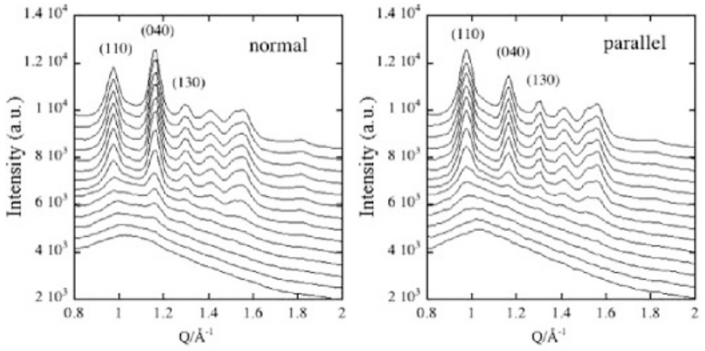

Figure 5. Time evolution of 1D WAXS profiles normal and parallel to the flow direction after cessation of the shear with shear rate of $70\,s^{-1}$. The profiles were shifted vertically for clarification. Annealing times after pulse shear are 0, 2, 4, 6, 8, 10, 15, 20, 25, 30, 35, 40, 45 and 50 min from bottom to top for both parallel and normal directions.

intensity was plotted in Figure 3 (lower) against logarithm of the shear rate. Although the data points are rather scattered, there certainly exists a critical shear rate for the anisotropy $\dot{\gamma}^*_{ani,WAXS}$ or for the crystal lattice formation in the kebab. Extrapolating the data to the degree of anisotropy of unity, we evaluated the critical shear rate $\dot{\gamma}^*_{ani,WAXS}$ to be $3.3 \pm 0.5\,s^{-1}$, which was larger than the critical shear rate for the reduction in the induction period $\dot{\gamma}^*_{ind,WAXS}$ ($\sim 1\,s^{-1}$), similar to the cases of the DPLS and SAXS experiments. The value of $3.3\,s^{-1}$ is rather close to the critical values for the anisotropic structure formations in DPLS ($= 3.1\,s^{-1}$) and in SAXS ($= 3.3\,s^{-1}$) ($\dot{\gamma}^*_{ani,DPLS} \approx \dot{\gamma}^*_{ani,SAXS} \approx \dot{\gamma}^*_{ani,WAXS} \approx 3.2\,s^{-1}$), suggesting that the anisotropic structure formation is dominated by a common origin. These values are larger than the critical shear rates for the induction period evaluated in DPLS, SAXS and WAXS measurements ($\dot{\gamma}^*_{ind,DPLS} \approx \dot{\gamma}^*_{ind,SAXS} \approx \dot{\gamma}^*_{ind,WAXS} \approx 1\,s^{-1}$). In the following we discuss the formation mechanism on the basis of these data.

Comparison of DPLS, SAXS and WAXS Data and Formation Mechanism of Shish-kebab Structure. The time evolutions of the scattering intensities were compared among the DPLS, SAXS and WAXS measurements. The intensities of DPLS, SAXS and WAXS were shown as a function of annealing time after applying pulse shear with shear rate of $70\,s^{-1}$ at 132 °C in Figure 6. It is very clear that the DPLS intensity rises up the earliest at around 20 s, and the SAXS intensity is next at 100 s and finally the WAXS intensity comes at around 140 s. When we compare intensities obtained by different scattering methods we have to take into account the difference of sensitivities. During the crystallization process at 132 °C under quiescent condition, we observed the onset of DPLS, SAXS and WAXS intensities at about 300 s, 650 s and 900 s, respectively. These onset times reflect the difference of the sensitivities involving structure factor, scattering contrast, counter efficiency, noise-

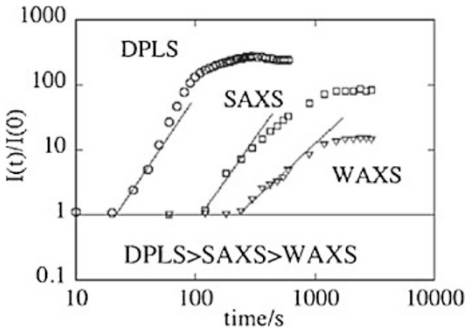

Figure 6. Comparison of time evolution of DPLS, SAXS and WAXS intensities during crystallization process of iPP at 132 °C after pulse shear with shear rate of $70\,s^{-1}$.

to-signal ratio, etc., and hence it is difficult to compare them directly. In order to compare the results, we took the ratio of the onset time under quiescent to that under shear for each scattering method, which gives 15 ($= 300/20$), 6.5 ($= 650/100$), 6.4 ($= 900/140$) for DPLS, SAXS and WAXS, respectively. The largest ratio of 15 indicates that the shish-like structure formation observed in DPLS is the most accelerated by shear, suggesting that the shish-like structure is formed first. The ratios for SAXS and WAXS are almost the same and smaller than for DPLS, meaning that the acceleration of the kebab structure formation by the flow is less than the shish-like structure. In other words, the shish-like structure is formed earlier than the kebab. On the other hand, it is very interesting to point out that the critical shear rate for the anisotropic structure formation is almost the same for DPLS, SAXS and WAXS, which are 3.1 ± 0.3, 3.3 ± 0.6 and $3.3 \pm 0.5\,s^{-1}$, respectively: $\dot{\gamma}^*_{ani,DPLS} \approx \dot{\gamma}^*_{ani,SAXS} \approx \dot{\gamma}^*_{ani,WAXS}$ ($\equiv \dot{\gamma}^*_{ani}$). How can we understand the results? The ratio of the onset times implies that the shish-like structure oriented along the flow is formed first, and then the lamella (kebab) may be epitaxially formed on the surface of shish-like structure, resulting in the oriented lamella structure or the kebab

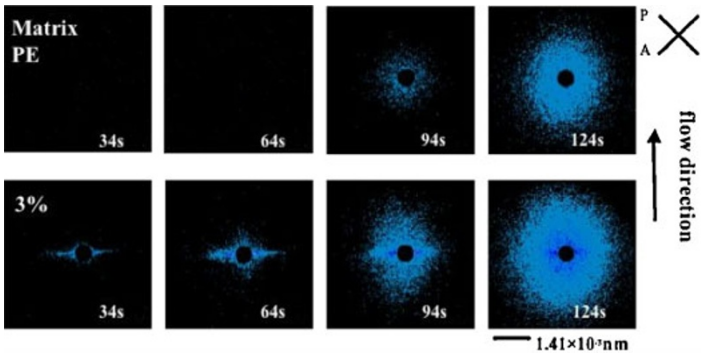

Figure 7. Time evolution of 2D DPLS patters for the matrix PE (LMW PE) and the PE blend including 3 wt % UHMW PE during the crystallization process at 129 °C after pulse shear. The shear rate and the strain were 4 s^{-1} and 1600%, respectively. (Reprinted from Ref. 27)

structure. If the oriented shish-like structure is not formed in the weak shear rate range below the critical value $\dot{\gamma}^*_{ani,DPLS}$, it would be impossible to form the oriented kebabs. In other words, the critical shear rate for the anisotropic shish-like structure formation governs the orientation of the kebab.

Next we consider why the critical shear rate for the reduction in induction time $\dot{\gamma}^*_{ind}$ is smaller than that for the anisotropic structure $\dot{\gamma}^*_{ani}$. In the low shear rate region below the critical value for the reduction in the induction time ($\dot{\gamma} < \dot{\gamma}^*_{ind}$), polymer chains are somewhat extended to orient by the shear. If crystallization occurs in the oriented state the crystallization rate must be faster than that under quiescent state. However, in the low shear rate rage we did not observe any acceleration of crystallization rate, suggesting that the orientation must relax to be isotropic before nucleation. In this case, crystallization occurs in isotropic melt and acceleration of crystallization would not be observed. In the shear rate region above the critical shear rate for the reduction in the induction time and below the critical shear rate for the anisotropic structure formation ($\dot{\gamma}^*_{ind} < \dot{\gamma} < \dot{\gamma}^*_{ani}$), crystal nucleation must occur before the relaxation of the orientation, and the nucleation rate is accelerated due to the orientation (orientation-induced crystallization). This acceleration is in a small orientation domain because the so-called primary nuclear is in a size of ~15 nm.[36] On the other hand, for the shish-like structure formation, the crystal growth must occur along the oriented chains or new crystal nuclei must be formed along the chains (or the segments) to prevent the relaxation of chain orientation. In this shear rate region, therefore, it is expected that the chain orientation is relaxed in global scale (~μm scale) before the crystal growth occurs along the chains. Above the critical shear rate for the anisotropic structure formation ($\dot{\gamma}^*_{ani} < \dot{\gamma}$), on the other hand, nucleation rate of polymer chains oriented by the shear is accelerated due to the orientation and the crystal growth in the large scale occurs before the relaxation of chain orientation, resulting in the anisotropic shish-like structure. The chain relaxation is mainly governed by reptation motion, suggesting that entanglements of polymer chains play an important role and the critical shear rate $\dot{\gamma}^*_{ani}$ is in the order of inverse of the reptation time. Folded chain lamella crystals (kebabs) grow on the surface of the shish to form the shish-kebab structure. It is expected that the kebab grows epitaxially on the surface of the shish-like structure, and hence the acceleration of the shish growth accelerates the kebab growth and the anisotropic shish-like structure induces the anisotropic kebab formation. Therefore, it is not surprising that the critical shear rates are almost identical between the kebab and shish-like structure for the reduction in the induction time as well as for the anisotropic structure formation.

Crystallization of Blends of Ultra-high and Low Molecular Weight Polyethylene

In this section we examine the effects of ultra-high molecular weight component in the crystallization of PE under shear flow, and we also study hierarchic structure of shish-kebab in a wide spatial scale using neutron scattering technique.

Depolarized Light Scattering. Figure 7 shows the time evolution of 2D DPLS patterns of the matrix PE (LMW PE) and the PE blend including 3 wt % UHMW one during the crystallization process at 129 °C after the pulse shear. The shear rate $\dot{\gamma}$ and the shear stain ε are 4 s^{-1} and 1600%, respectively. In the case of the matrix PE an isotropic scattering pattern appears at around 80 s after applying the pulse shear and increases in intensity with annealing time. On the other hand, the 3% blend shows a very sharp streak-like scattering normal to the flow direction, which appears at around 30 s after the pulse shear, corresponding to the shish-like structure in μm scale. It is called the *row structure* hereafter. At about 80 s in the late stage, isotropic scattering appears to cover the

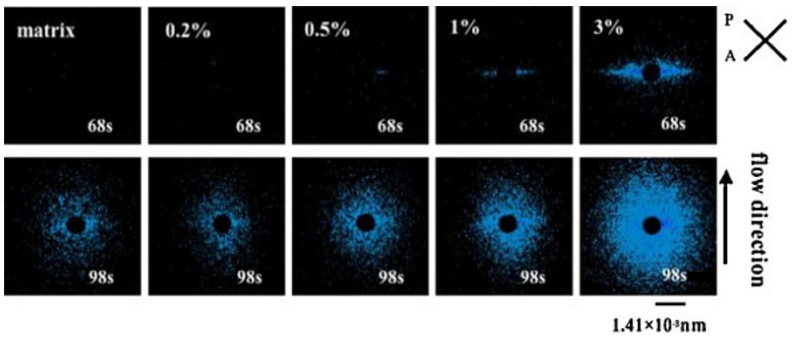

Figure 8. 2D DPLS patters of the PE blends with various concentrations of the UHMW PE from 0 to 3 wt % at 68 and 98 s after pulse shear. The shear rate and the strain were $4\,s^{-1}$ and 1600%, respectively. (Reprinted from Ref. 27)

anisotropic one. It is evident that the streak-like scattering is due to the UHMW PE because the matrix PE does not show any anisotropic scattering under this shear condition. From these observations, we can directly conclude that the UHMW component enhances the formation of the *row structure*.

We also examined the effects of the concentration of the UHMW PE C_{HMPE}. Figure 8 shows the 2D scattering patterns of the PE blends at 68 and 98 s after the pulse shear as a function of the concentration C_{HMPE}. The shear rate and the shear strain are $4\,s^{-1}$ and 3200%, respectively. Anisotropic scattering patterns are not observed when the concentration C_{HMPE} of the UHMW PE is less than 0.5 wt %. At around $C_{\mathrm{HMPE}} = 0.5$ wt %, a very weak anisotropic scattering is observed at 68 s after the pulse shear as seen in Figure 8 and the 2D scattering intensity increases in the anisotropy with the concentration C_{HMPE}, suggesting that there is a critical concentration C^*_{ani} for the anisotropic scattering at around $C_{\mathrm{HMPE}} = 0.5$ wt %. In Figure 9, the degree of anisotropy R_{ani} at 68 s after the pulse shear is plotted against the concentration of the UHMW PE C_{HMPE} for three shear conditions, under which the matrix PE does not show the anisotropic scattering pattern. It is obvious that the degree

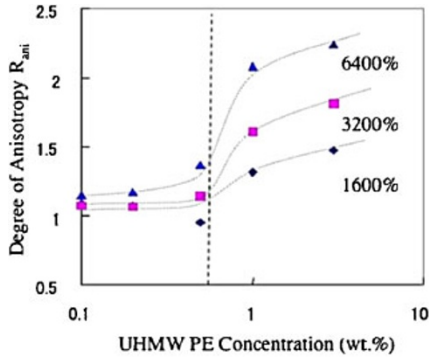

Figure 9. Degree of anisotropy as a function of the concentration of UHMW PE for various shear strains 1600, 3200 and 6400%. Shear rate was $4\,s^{-1}$. (Reprinted from Ref. 27)

of anisotropy is almost unity below $C_{\mathrm{HMPE}} =$ 0.5–0.6 wt % while it abruptly increases above this concentration, showing that the critical concentration for the anisotropy C^*_{ani} is 0.5–0.6 wt %. We compare the critical concentration C^*_{ani} to the chain overlap concentration C^*_{Rg} of the UHMW PE. The overlap concentration C^*_{Rg} was calculated taking into account the molecular weight distribution[37] to be 0.178 g/cm^3 or 0.209 wt %. The ratio of the critical concentration to the overlap concentration C^*_{ani}/C^*_{Rg} is 2.5–3. This strongly suggests that entanglements of the UHMW PE are very important for the formation of the *row structure*. This result may be understood in the following picture. In order to produce the *row structure* or the precursor of shish polymer chains must be extended due to the shear. Suppose that the UHMW PE are isolated in the blend, they are somewhat extended by the shear flow, however it does not lead to the anisotropic structure formation. On the other hand, when the concentration of UHMW PE is above the critical value for the entanglements, the chains must be extended due to the connectivity as polymer network is deformed. The critical concentration for the anisotropy C^*_{ani} must correspond to the critical concentration for the effective entanglements. This is schematically illustrated in Figure 10(a) and 10(b). These pictures remind us the gel spinning technique[38–41] to produce ultra-high strength and ultra-high modulus fiber of PE although all of the situations are not the same. In this procedure, PE chains are extremely extended because the tension is transmitted though the cross-linking points in the gel network. On the other hand, in order to obtain the ultra-high strength fiber the number of the cross-linking points should be as little as possible because too many cross-linking points prevent the extension of polymer chains. It is therefore expected in the crystallization of the PE blend under the shear that the formation of the *row structure* or the precursor of shish is depressed at a rather high concentration of the UHMW PE above C^*_{ani} because the polymer chains cannot be extended

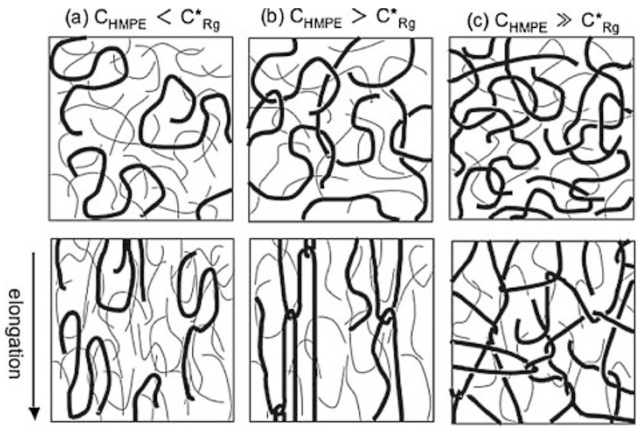

Figure 10. Schematic illustrations of the role of UHMW PE in formation of *row structure*. Thin and thick curves represent UHMW and LMW PEs, respectively. (a) $C_{HMPE} < C^*_{Rg}$: UHMW PE chains are isolated and slightly extended by the shear, (b) $C_{HMPE} > C^*_{Rg}$: UHMW PE chains are entangled and extended due to the connectivity as polymer network is deformed, (c) $C_{HMPE} \gg C^*_{Rg}$: too many cross-linking points (or entanglements) prevent extension of UHMW PE chains. (Reprinted from Ref. 27)

due the shear because of too many entanglements as illustrated in Figure 10(c).

Small-angle X-ray Scattering. In order to see formation of kebab we performed small-angle X-ray scattering (SAXS) measurements on crystallization process of the PE blends under the same shear condition as that in DPLS measurements. In the SAXS experiments the pulse shear was applied at 30 °C above the crystallization temperature T_c. Figure 11 shows an example of time evolution of 2D SAXS profiles for the PE blends including 0, 1 and 2 wt % UHMW PE during the crystallization process at $T_c = 132$ °C after applying shear flow. In the case of 0 wt %, only isotropic scattering patterns are observed. On the other hand, the 1 and 2 wt % blends show two-spot scattering parallel to the shear direction and the spots became stronger in intensity with annealing time, showing that the UHMW PE enhances the anisotropic structure formation. These orientated features must be due to the kebab structures, which are oriented perpendicularly to the shear direction, and the spot position corresponds to the so-called long period between kebabs. The present results suggest that the UHMW PE also enhances the kebab structure formation and there is a critical concentration for the kebab formation.

We also examined the crystallization temperatures T_c dependence of the time-resolved SAXS data. Figure 12 shows the time evolution of 2D SAXS images of the PE blend with UHMW PE concentration of 0.2 wt % for various crystallization temperatures T_c. In a temperature range below about 127 °C two strong spots parallel to the shear direction are observed after a certain induction time and followed

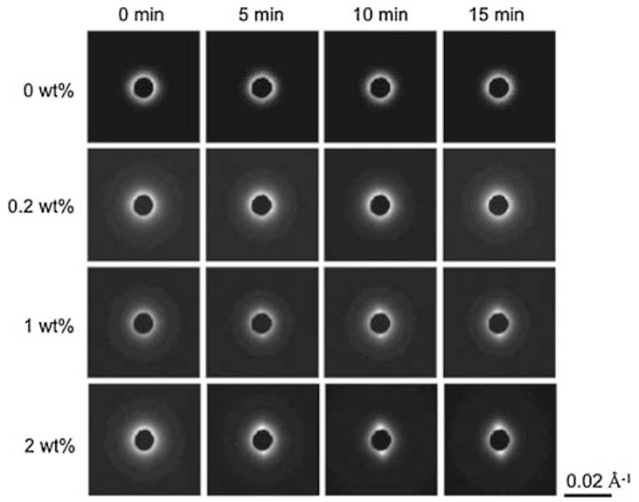

Figure 11. Time evolution of 2D SAXS patterns during crystallization process of PE blends with UHMW PE concentration of 0, 0.2, 1 and 2 wt % at crystallization temperature 132 °C.

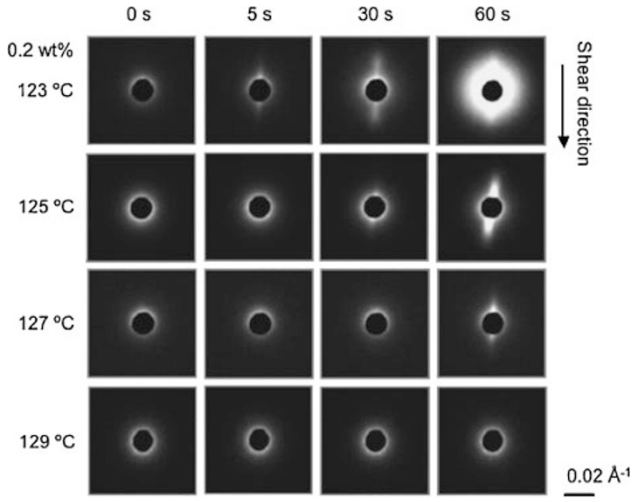

Figure 12. Time evolution of 2D SAXS patterns during crystallization process of PE blends with UHMW PE concentration of 0.2 wt % at various crystallization temperatures, 123, 125, 127 and 129 °C.

by isotropic scattering due to the spherulite formation. As the crystallization temperature decreases, the onset time of the anisotropic scattering becomes shorter. This is due to the increase in degree of super-cooling (or quenching depth), which is a driving force of crystallization in this temperature region.[42] On the other hand the spot scattering parallel to the shear direction is not observed above about 129 °C, at least during the annealing period of 1 h. Note that the two spots were observed even above ~129 °C for the concentrations of UHMW PE higher than 0.2 wt %, showing that the critical UHMW PE concentration for the anisotropy exists and depends on the crystallization temperature.

We have evaluated the critical UHMW PE concentration C^*_{SAXS} for the anisotropy as a function of crystallization temperature. The critical UHMW PE con-

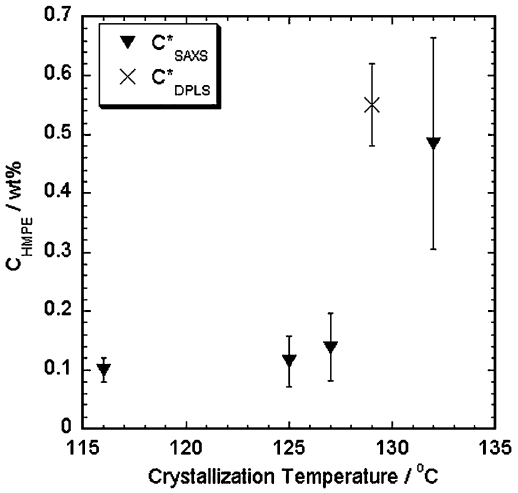

Figure 13. Critical concentration C^*_{SAXS} of UHMW PE for anisotropy in SAXS pattern against crystallization temperature T_c. Filled square shows critical concentration C^*_{ani} for anisotropic structure formation in DPLS.

centration C^*_{SAXS} thus obtained is plotted against the crystallization temperature in Figure 13. In the previous section we showed that the critical concentration for the *row structure* or the precursor of shish was about 0.5–0.6 wt % at $T_c = 132\,^\circ$C, which was almost identical with the C^*_{SAXS} value determined from the kebab formation. This result supports the idea that the entanglements of UHMW PE also play an important role in kebab formation. In this experiment, on the other hand, we observed that the critical concentration C^*_{SAXS} decreased with the crystallization temperature T_c, and reached a constant value of $\sim$0.1 wt %, which was about half of the chain overlap concentration C^*_{Rg}. Does this result mean that the critical concentration is not related to entanglements? Seki *et al.*[32] studied a critical concentration for the anisotropic structure formation in isotractic polypropylene blend including small amount of UHMW component and found that it was lower than the overlap concentration C^*_{Rg}, similar to the present result at the low crystallization temperatures below about 127 °C. In order to understand their results and our results we have to consider the molecular weight distribution of UHMW PE. The longer chains in UHMW PE could be entangled at lower concentration than that for the average molecular weight, and hence more oriented than the shorter ones. Therefore, the lower critical concentration than the overlap concentration is not so surprising for polymers with molecular weight distribution. As for the crystallization temperature dependence of the critical concentration may suggest that the anisotropic structure formation is determined by a competition between the orientation relaxation of polymer chain and the crystallization (nucleation) rate. The detailed discussions will be given in a forthcoming paper.

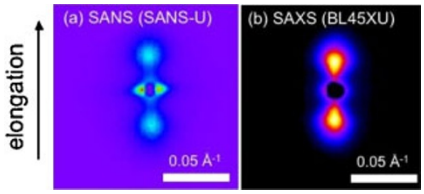

Figure 14. 2D SANS (a) and SAXS (b) patterns of elongated PE blend of low molecular weight deuterated PE (LMW d-PE) and ultra-high molecular weight hydrogeneated polyethylene (UHMW h-PE). Weight fraction of UHMW h-PE is 2.8%.

Small-angle Neutron Scattering. In the DPLS measurements we showed that the *row structure* or the precursor of shish had a diameter in μm scale. On the other hand, as mentioned in Introduction, TEM observations showed that shish (extended chain crystal) had a diameter of $\sim$10 nm.[7–10] These observations suggest that shish-kebab has hierarchic structure in a wide spatial scale. In this work we studied the hierarchic structure using small-angle neutron scattering in a very wide Q range.[43]

We used hydrogen/deuterium (H/D) labeling method in SANS. It is well known in SANS that the scattering contrast between *hydrogenated* and *deterated* PEs is very large,[44] so that if the *row structure* is formed from UHMW h-PE we could observe it due to the high scattering contrast. For this purpose we used an elongated blend of UHMW h-PE and LMW d-PE (2.8/97.2), and performed SANS and SAXS measurements. In the SANS data in Figure 14(a) we clearly see the streak-like scattering normal to the elongation direction in addition to the two-spot pattern along the elongation direction. The former and the latter must correspond to the *row structure* and the kebab structure (or kebab spacing). On the other hand, we only see the two-spot pattern along the elongation direction in the SAXS result (Figure 14(b)), corresponding to the kebab structure. The results directly show that the *row structure* is mainly formed from the UHMW h-PE although the Q range is not enough to estimate the form factor of the *row structure*. In order to evaluate the form factor we have extended the Q range in this work using F-SANS and SWAN spectrometers. Combining all the data we have plotted the 1D scattering intensities in the parallel and normal directions in Figure 15 in a Q range of 4×10^{-4} to 3 Å^{-1}.

The SANS contrast in the present sample arises from two causes: scattering length density difference due to mass density difference and scattering length difference between H and D. We assume that the mass density correlation function and the H/D density correlation function could be decoupled because the fraction of UHMW h-PE is very small (2.8 wt %). In

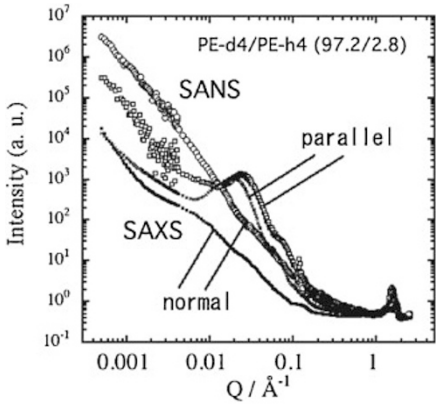

Figure 15. 1D SANS and SAXS profiles of elongated PE blend of LMW d-PE and UHMW h-PE in directions normal and parallel to the elongation direction.

SAXS measurements h-PE and d-PE cannot be distinguished, and the scattering contribution due to the mass density fluctuations $I_{den}(Q)$ can be observed in SAXS. Therefore, in order to evaluate the scattering contribution due to the mass density fluctuations $I_{den}(Q)$ we carried out WAXS, SAXS and U-SAXS measurements on the same sample, and the results are plotted in Figure 15 together with the neutron data where the WAXS intensity was adjusted so that the intensity ratio of WAXS to WANS is equal to the calculated one. The difference intensities are plotted in Figure 16. The difference intensities approximately correspond to the form factors of the *row structure*.

We have first employed a cylinder model to describe the form factor of the *row structure*. The form

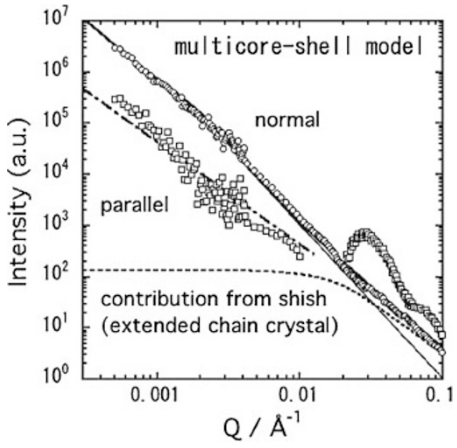

Figure 16. 1D SANS difference intensities in directions normal and parallel to the elongation direction after subtraction of contributions of density fluctuations which were evaluated from SAXS data. Thick solid lines are the results of fit to multicore-shell cylinder model and thin chain line is a contribution of the core [or the shish (extended chain crystal)]. Thick dotted line is the result of fit to the cylinder model.

factor of an oriented cylinder with a length of $2H$ and radius of R has been reported by Shibayama *et al.*[45] According to the report we have calculated the form factor in the normal direction, and fitted to the observed scattering intensity after convoluted with the resolution functions of the spectrometers. The result of fit is shown by a dotted line in Figure 16, which is almost behind the data points (or a thick line) in the Q range below about $0.02\,\text{Å}^{-1}$. This means that the cylinder model can describe the *row structure* only in the large scale above about 300 Å, and the evaluated radius was $\sim$1 μm. This large radius certainly is not an extended chain crystal because it is large enough to include kebab inside, but it must be the bundle of the shish-kebab. In the Q range above about $0.02\,\text{Å}^{-1}$, on the other hand, the observed data in the normal direction show excess scattering, suggesting some extra structure which is not included in the cylinder model. As mentioned in the Introduction, Keller and coworkers[7–10] reported shish structure with diameter of $\sim$10 nm, which must correspond to extended chain crystal (the shish). We have assigned the excess scattering intensity above about $0.02\,\text{Å}^{-1}$ to the shish structure. In order to describe this contribution we employed a multicore-shell cylinder model, in which the core and shell describe the extended chain crystal (the shish) and the *row structure* in μm scale, respectively. Calculating the scattering intensity of the multicore-shell cylinder model we fitted to the observed one in the normal direction. The result of the fit was shown by a thick solid line in Figure 16 where the core contribution was also indicated by a chain line. The fitness is very good, showing that the present model, which is termed multicore-shell cylinder model, is appropriate to describe the shish structure and the *row structure*. The evaluated radii of the shell and core are $\sim$1 μm and 4.5 nm, respectively, and the number of core cylinders is about 3, meaning that only 3 extended chain crystals are in the *row structure*. This very small number of the shish is one of the reasons why we did not observe the extended chain crystals in SAXS measurements. The results provide us a picture that the *row structure* with radius of $\sim$1 μm includes about 3 extended chain crystals (shish) with diameter of 4.5 nm. The *row structure* must a bundle of the shish-kebab structure. If we assume that the three shish-kebab structure equally shear the large bundle (or the *row structure*) with radius of $\sim$1 μm, the radius of the kebab would be about 500 nm. Calculating the intensity in the parallel direction we have estimated the length of the cylinder $2H$ to be $\sim$12 μm. This length is comparable to that of the shish observed by Keller and coworkers by TEM.[7–10] The *row structure* evaluated in the SANS study was schematically illustrated in Figure 17.

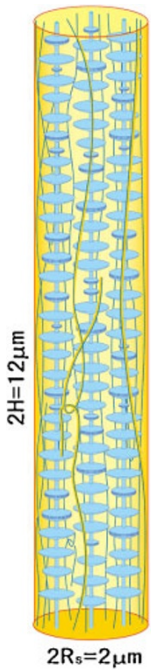

Figure 17. Schematic representation of the *row structure* including three shish (extended chain crystals). The row structure is a bundle of shish kebab surrounded by the elongated network of ultra-high molecular weight component.

In the previous section we found that the *row structure* or the precursor of shish in μm scale appeared in a very early stage of crystallization. This precursor is very similar to the *row structure* in size observed here for the elongated PE. We also found that the *row structure* or the precursor formation was enhanced by addition of high molecular weight component above a certain critical concentration, suggesting that entanglements of high molecular weight component play an important role for the *row structure* formation. In other words, the *row structure* is formed from deformation of polymer network due to entanglements, and hence we proposed a gel-spinning-like formation mechanism for the *row structure* in a previous section. Recent experiment on isotactic polystyrene (iPS) showed that *row structure* (precursor) in μm scale aligned along the shear flow appeared even above the nominal melting temperature T_m.[46] In the SANS experiment, it was shown that the elongated PE has *row structure* similar to the precursor although the crystallization mechanism is very different between the pulse shear crystallization and the elongation crystallization. The finding may imply that the network of UHMW PE due to entanglements play an important role for the *row structure* formation in both the crystallization processes. The large oriented network (or the *row structure*) may enhance the formation of the shish structure (or the extended chain crystal).

CONCLUSION

In this article we reviewed our recent progress of the studies on polymer crystallization under flows using the so-called quantum beam technology such as time-resolved depolarized light scattering (DPLS), time-resolved small-angle and wide angle X-ray scattering (SAXS and WAXS) and small-angle neutron scattering (SANS). In the experiments on iPP we observed the structure formation process of the shish-like structure (or the *row structure*) in micrometer scale, the kebab in tens nm scale and the crystalline lattice in nm scale, focusing effects of the shear rates and the shear strain. The results suggested that the shish-like structure (or the *row structure*) was first formed and the kebab grew on the surface of the shish or the shish-like structure, and hence the critical shear rate for the anisotropic structure formation was dominated by the shish formation. Effects of high molecular weight component of PE were examined using a blend including 2.8 wt % of ultra-high molecular weight (UHMW) PE with $M_w = 2{,}000{,}000$. It was found that the *row structure* formation was enhanced by the addition of UHMW PE above a critical concentration of 0.5–0.6 wt % at 129 °C. The critical concentration depended on the crystallization temperature, implying that the formation of the shish-like structure or the *row structure* was dominated by a competition between the crystallization rate and the chain relaxation rate. SANS study on an elongated PE blend with deuterium labeling method revealed that a long cylindrical object 2 μm in diameter and 12 μm in length was formed from the deformed network of UHMW chains, which included three shishs or extended chain crystals inside. The long cylindrical object was very similar to the *row structure* observed in DPLS during crystallization process under shear flow, suggesting that the network of UHMW PE due to entanglements played an important role for the *row structure* formation in both elongational crystallization as well as shear induced crystallization.

REFERENCES

1. I. M. Ward, in "Structure and Properties of Oriented Polymers," Wiley, New York, 1975.
2. A. Ziabicki, in "Fundamentals of Fiber Formation," Wiley, New York, 1976.
3. Z. K. Walczak, in "Processes of Fiber Formation," Elsevier, Amsterdam, 2002.
4. A. Keller and J. W. H. Kolnaar, in "Processing of Polymers," H. E. H. Meijer, Ed. VCH, New York, 1997, p. 189.
5. A. J. Pennings and A. M. Kiel, *Colloid. Z. Z. Polym.*, **205**, 160 (1965).

6. A. J. Pennings, *J. Polym. Sci., Part C: Polym. Symp.*, **59**, 55 (1977).
7. J. A. Odell, D. T. Grubb, and A. Keller, *Polymer*, **19**, 671 (1978).
8. Z. Bashir, J. A. Odell, and A. Keller, *J. Mater. Sci.*, **19**, 3713 (1984).
9. A. Keller and J. A. Odell, *Colloid Polym. Sci.*, **261**, 181 (1985).
10. Z. Bashir, J. A. Odell, and A. Keller, *J. Mater. Sci.*, **21**, 3993 (1986).
11. Z. Bashir, M. J. Hill, and A. Keller, *J. Mater. Sci. Lett.*, **5**, 876 (1986).
12. J. M. Samon, J. M. Schultz, B. S. Hsiao, S. Seifert, N. Stribeck, I. Gurke, G. Collins, and C. Saw, *Macromolecules*, **32**, 8121 (1999).
13. J. M. Samon, J. M. Schultz, J. Wu, B. S. Hsiao, F. Yeh, and R. Kolb, *J. Polym. Sci., Part B: Polym. Phys.*, **37**, 1277 (1999).
14. R. H. Somani, B. S. Hsiao, A. Nogales, S. Srinivas, A. H. Tsuo, I. Sics, J. Balta-Calleja, and T. A. Ezquerra, *Macromolecules*, **33**, 9385 (2000).
15. J. M. Schultz, B. S. Hsiao, and J. M. Samon, *Polymer*, **41**, 8887 (2000).
16. J. M. Samon, J. M. Schultz, B. S. Hsiao, J. Wu, and S. Khot, *J. Polym. Sci., Part B: Polym. Phys.*, **38**, 1872 (2000).
17. J. M. Samon, J. M. Schultz, B. S. Hsiao, S. Khot, and H. R. Johnson, *Polymer*, **42**, 1547 (2001).
18. A. Nogales, R. H. Somani, B. S. Hsiao, S. Srinivas, A. H. Tsuo, J. Balta-Calleja, and T. A. Ezquerra, *Polymer*, **42**, 5247 (2001).
19. R. H. Somani, B. S. Hsiao, A. Nogales, H. Fruitwala, S. Srinivas, and A. H. Tsuo, *Macromolecules*, **34**, 5902 (2001).
20. R. H. Somani, L. Young, B. H. Hsiao, P. K. Agarwal, H. A. Fruitwala, and A. H. Tsuo, *Macromolecules*, **35**, 9096 (2002).
21. R. H. Somani, L. Yang, and B. S. Hsiao, *Physica A* **304**, 145 (2002).
22. L. Yang, R. H. Somani, I. Sics, B. H. Hsiao, R. Kolb, H. Fruitwala, and C. Ong, *Macromolecules*, **37**, 4845 (2004).
23. N. V. Pogodina, S. K. Siddiquee, J. W. v. Egmond, and H. H. Winter, *Macromolecules*, **32**, 1167 (1999).
24. N. V. Pogodina, V. P. Lavrenko, S. Srinivas, and H. H. Winter, *Polymer*, **42**, 9031 (2001).
25. A. Elmoumni, H. H. Winter, A. J. Waddon, and H. Fruitwala, *Macromolecules*, **36**, 6453 (2003).
26. H. Fukushima, Y. Ogino, G. Matsuba, K. Nishida, and T. Kanaya, *Polymer*, **46**, 1878 (2005).
27. Y. Ogino, H. Fukushima, G. Matsuba, N. Takahashi, K. Nishida, and T. Kanaya, *Polymer*, **47**, 5669 (2006).
28. Y. Ogino, H. Fukushima, N. Takahashi, G. Matsuba, K. Nishida, and T. Kanaya, *Macromolecules*, **39**, 7617 (2006).
29. G. Kumaraswamy, A. M. Issaian, and J. A. Kornfield, *Macromolecules*, **32**, 7537 (1999).
30. G. Kumaraswamy, R. K. Verma, A. M. Issaian, P. Wang, J. A. Kornfield, F. Yeh, B. Hsiao, and R. H. Olley, *Polymer*, **41**, 8934 (2000).
31. G. Kumaraswamy, J. A. Kornfield, F. Yeh, and B. Hsiao, *Macromolecules*, **35**, 1762 (2002).
32. M. Seki, D. W. Thurman, J. P. Oberhauser, and J. Kornfield, *Macromolecules*, **35**, 2583 (2002).
33. T. Fujisawa, K. Inoue, T. Oka, H. Iwamoto, T. Uruga, T. Kumasaka, Y. Inoko, N. Yagi, M. Yamamoto, and T. Ueki, *J. Appl. Crsytallogr.*, **33**, 797 (2000).
34. Y. Ito, M. Imai, and S. Takahashi, *Physica B* **213/214**, 889 (1995).
35. T. Otomo, M. Furusaka, S. Satoh, T. Itoh, S. Adachi, M. Shimizu, and M. Takeda, *J. Phys. Chem. Solids*, **60**, 1579 (1999).
36. B. Wunderlich, in "Macromolecular Physics—Crystal Nucleation, Growth, Annealing," Academic Press, New York, 1976.
37. R. C. Oberthuer, *Makromol. Chem.*, **179**, 2693 (1978).
38. P. Smith, P. J. Lemstra, B. Kalb, and A. J. Pennings, *Polym. Bull.*, **1**, 733 (1979).
39. P. Smith and P. J. Lemstra, *J. Mater. Sci.*, **15**, 505 (1980).
40. P. J. Lemstra, N. A. J. M. V. Aerle, and C. W. M. Bastiaansen, *Polym. J.*, **19**, 85 (1987).
41. C. W. M. Bastiaansen, *J. Polym. Sci., Polym. Phys. Ed.*, **28**, 1475 (1990).
42. L. Mandelkern, in "Crystallization of Polymers—Kinetics and Mechanisms," Cambridge Univesity Press, Cambridge, 2002.
43. T. Kanaya, G. Matsuba, Y. Ogino, K. Nishida, H. Shimizu, T. Shinohara, T. Oku, J. Suzuki, and T. Otomo, *Macromolecules*, **40**, 3650 (2007).
44. G. E. Bacon, in "Neutron Diffraction," Clarendon Press, Oxford, 1975.
45. M. Shibayama, S. Nomura, T. Hashimoto, and E. L. Thomas, *J. Appl. Phys.*, **66**, 4188 (1989).
46. T. Kanaya, Y. Takayama, Y. Ogino, G. Matsuba, and K. Nishida, in "Progress in Understanding of Polymer Crystallization, Lecture Notes in Physics," G. Reiter, and G. Strobl, Ed., Springer, Berline, 2006, p 91.

Toshiji KANAYA was bone in Osaka, in 1953, and graduated from the Department of Polymer Chemistry of Kyoto University, and awarded Master of Engineering in 1978 and Doctor of Engineering in 1981 at the same university. He was appointed to instructor in Institute for Chemical Research, Kyoto University in 1982 and to associate professor in 1989, and promoted to a professor in 2003. During the period, he was a visiting scientist in Imperial College in London in 1986 and stayed in Max Planck Institute for Polymer Research, Mainz, from 1991 to 1992 as a Humboldt Fellow. He was awarded the Fiber Society Award in 2002 and the Polymer Science Award in 2007. His current research interests are hierarchic structure and dynamics in polymer crystallization, polymer glass transition and polymer gelation.

Go MATSUBA was born in Aichi, Japan, in 1973, and graduated from the Department of Polymer Chemistry of Kyoto University, Kyoto, Japan in 1996. He studied polymer physics and awarded Master of Engineering in 1998 and Ph. D (Engineering) in 2001 at the same university. He was a guest postdoctoral researcher at Polymers Division in National Institute of Standards and Technology (NIST), USA from 2001 to 2003. He joined the 21st century COE program, Kyoto University Alliance for Chemistry, as a postdoctoral researcher in 2003. He was appointed assistant professor at the Institute for Chemical Research, Kyoto University in 2004. His research interests are the crystallization and phase separation of polymer/polymer blends in various external fields with scattering methods and microscopy.

Yoshiko OGINO was born in Aichi, Japan, in 1977, and graduated from the Undergraduate school of Engineering of Kyoto University, Kyoto, Japan in 2001. She studied polymer crystallization and awarded Master Engineering in 2003 and Doctor of Philosophy in Engineering in 2006 at the same university. She studies the density fluctuation of polymers under deformation at Kyoto University as a postdoctoral fellow.

Nobuaki TAKAHASHI was born in Osaka, Japan, in 1976, and graduated from the Faculty of Engineering, Kyoto University, Kyoto, Japan in 1999. He studied polymer science and awarded Master of Engineering in 2001 and Doctor of Engineering in 2004 at the same university. He was appointed scientist at the J-PARC (Japan Proton Accelerator Research Complex) Center of Japan Atomic Energy Agency in 2007.

Koji NISHIDA was born in Hyogo, Japan, in 1959, and graduated from Department of Polymer Chemistry, Kyoto University in 1984. He studied polymer physics and awarded Master of Engineering in 1986. He was appointed assistant professor at Department of Nuclear Engineering, Hokkaido University in 1986, assistant professor at Institute for Chemical Research, Kyoto University in 1990 and promoted to associate professor in 2004 at the same University. During this period he received Ph. D. from Kyoto University in 2001. His current interests are the crystallization of polymers and the structure of polyelectrolyte solutions.